# Chapter 2
# Flavor as a Probe for Non-SM Physics

*This chapter introduces the motivations for the measurement described in this thesis. After a brief description of the general theoretical framework we focus on CP violation in $B_s^0 - \bar{B}_s^0$ mixing through $B_s^0 \to J/\psi\phi$ decays as probe for non-standard model physics. An overview of the measurement, and a summary of the current experimental status are also presented.*

## 2.1 The Current Landscape

The standard model (SM) of particle physics provides a quantum field theoretical description of three fundamental interactions, namely the strong, weak, and electromagnetic interactions, that act among the elementary spin-half particles, the quarks and the leptons [1]. The SM structure is based on symmetries of the Lagrangian for transformations of a gauge group, resulting in interactions being mediated by spin-one force carriers: eight massless gluons for the strong interaction; two charged massive bosons, $W^{\pm}$, and a single neutral massive boson, $Z^0$, for the weak interaction; and a massless photon, $\gamma$, for the electromagnetic interaction. Finally, the SM includes a spin-zero particle, the Higgs boson, which is the scalar excitation of the field that provides generation of particles masses through the spontaneous symmetry breaking of the gauge group of the electroweak interaction. Quarks and leptons interact via Higgs-mediated interactions that, unlike gauge interactions, are not ruled by symmetry principles. These *Yukawa* interactions are responsible for *flavor* physics. The term flavor is used to differentiate among the variety of species of quarks and leptons that have same quantum charges: up-type quarks ($u$, $c$, $t$), down-type quarks ($d$, $s$, $b$), charged leptons ($e$, $\mu$, $\tau$), and neutrinos ($\nu_e$, $\nu_\mu$, $\nu_\tau$), each featuring three flavors.

In July 2012, the CMS and ATLAS Collaborations at the Large Hadron Collider (LHC) announced the discovery of a resonance produced in proton–proton collisions [2, 3]. The new particle has a mass of approximately 125 GeV/c$^2$, with



S. Leo, *CP Violation in $B_s^0 \to J/\psi\phi$ Decays*, Springer Theses,
DOI 10.1007/978-3-319-07929-5_2

properties compatible with the SM Higgs interpretation. The discovery of the Higgs boson completes the validation of the SM, as an extremely predictive theory capable of accurately explaining most of the experimental phenomena probed so far [4]: we know today that the physics of fundamental particles and interactions at energies in the sub-eV-TeV range is successfully described by this theory.

However, a number of solid theoretical arguments, and some experimental results motivate a prejudice that the SM should be a low-energy restriction of a more general theory that includes additional particles and interaction couplings. For instance, classical gravity, well described by general relativity, should break down at energy scales close to $10^{19}$ GeV, the Planck scale, at which quantum effects of gravity should become relevant [5]. The SM would be necessarily invalidated at such energy calling for a theory of quantum gravity to integrate the SM at the Planck-scale energies. In addition, the calculation of the Higgs-boson mass is affected by divergences due to radiative corrections that invalidate the SM at an energy scale that depends on the mass itself. This energy scale represents the *cut-off* of the effective model, i.e., the energy above which the model needs likely to be extended by a more fundamental theory. Either a fine-tuning of the model parameters that can push the cut-off at the Planck scale, or non-SM particles whose virtual contributions eliminate the divergence were proposed [6]. The observed value of the Higgs-boson mass consolidates the SM at the electroweak scale, and moves the cut-off at larger energy [4]. Hence, the question if non-SM particles are present in the energy range from $\mathcal{O}(1)$ TeV to the Planck scale is open, motivated also by cosmological arguments based on a large mismatch between the quantity of baryonic and luminous matter in the universe and astrophysical observations [7].

## 2.2 Flavor as a Probe of Non-SM Physics

Non-SM particles can be produced *directly* in high-energy collisions and observed through their decay products, provided that the available center-of-mass energy is sufficient to produce the heavy particles with sensible rates. The heavier are particles that can be produced, the higher the physics scale probed. The reach of this *direct* approach crucially depends on the unknown energy scale of the non-SM physics particles. Pushing forward the energy frontier requires devising technologies to achieve ever-higher center-of-mass energies. However, the non-SM particles can become directly observable at energies not reachable with current and foreseen technology.

A complementary approach is to infer the presence of non-SM particles *indirectly* in processes where they could be virtually exchanged between SM particles, by detecting deviations of observables from expectations precisely calculated in the SM [8, 9]. In indirect searches, the production threshold energy is not as critical as in direct searches. Because quantum effects become smaller the heavier are the virtual particles at play, higher non-SM physics scales are explored by increasing the precision of the measurements while controlling the SM contributions with sufficient accuracy to identify unanbiguosly non-SM effects.

The flavor physics of quarks is among the most promising sector for indirect searches. Experimental access to a plethora of precisely measurable processes, along with a mature phenomenology that provides many accurate predictions, allows the redundant determination of several SM parameters that can be compared for precision tests of the overall picture [10]. Indeed, flavor physics has proved very successful in building the current understanding of particle physics. For instance, the theoretical *ansatz* to explain [11] the suppressed decay rate of quark transitions that change the strangeness flavor by two units (such as $K^0 \to \mu^+\mu^-$ decays) was crucial to postulate the existence of a then-unknown charm quark and estimate its mass, before its experimental discovery [12, 13]. Similarly, an important prediction of the large value of the top-quark mass before its direct observation [14, 15], was inferred from the indirect constraints imposed by the measurements of $B^0 - \bar{B}^0$ mesons oscillations [16].

The physics of flavor is the physics of matter at its most fundamental level. It consists in the study of underlying patterns in the family replications of quarks and leptons, and in the highly hierarchical structure of their masses and couplings. The flavor sector of the SM accounts for 10 out 18 free parameters of the theory and still is impressively predictive and peculiar. Flavor violation is allowed only in the quark sector. Weak interactions mediated by $W^\pm$ bosons that change flavor of quarks (flavor-changing charged-currents, FCCC) are universal; flavor transitions mediated by neutral currents (flavor-changing neutral-currents, FCNC) are highly suppressed. The last cannot occur at *tree-level*, i.e., through the mediation of a $W$ boson only, but they do require the intermediate exchange of a quark and a $W$ boson (*loop* transition). In Fig. 2.1 we show this features with two examples of Feynman diagrams representing the two flavor-changing transitions in terms of the elementary particles involved. The FCNC are further suppressed in the SM by the Glashow-Illiopoulos-Maiani (GIM) mechanism [11], namely the smallness of the mass differences between second- and first-generation quarks, and by the hierarchical structure of *quark-mixing* angles, which determines the rotation of the quark-flavor basis with respect to the

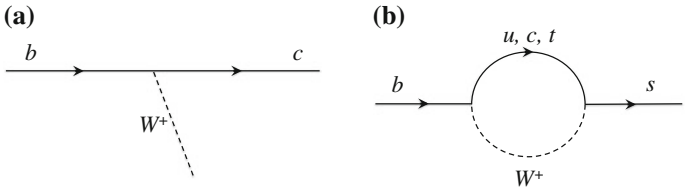


**Fig. 2.1** Feynman graphs of two examples of flavor transition of the $b$ quark. In **a**, the *tree*-level transition $b \to c$, where the $b$ quark changes flavor and charge $(-1/3)$ becoming a $c$ quark (with charge $+2/3$) through emission of a $W^+$ boson; in **b**, the *loop*-mediated transition $b \to s$, where the $b$ quark changes its flavor by exchanging an up-type quark (either $u$, or $c$, or $t$) and a $W$ boson with the $s$ quark. In this case, the charge of the initial quark and the charge of the final quark are the same. Tree-level transition involves quarks of different type (up-down and down-up), while loop-mediated transitions can change the flavor of two quarks of the same type (up-up and down-down)

weak-interaction basis. These phenomenological features determine the observed pattern of quark transitions, and any extension of the SM must account for them.

A generic effective-theory approach [8] is powerful for describing non-SM physics effects in flavor physics, in a model-independent way. Assuming the non-SM physics scale to be higher than the electroweak energy scale, non-SM physics effects can be described by a generalization of the Fermi theory. In this approach, the SM Lagrangian is included in a more general local Lagrangian, which includes a series of operators with dimension $d > 4$, $O_i^{(d)}$, constructed in terms of SM fields, with arbitrary couplings $c_i^{(d)}$ suppressed by inverse powers of an effective scale $\Lambda$, which represents the cut-off of the effective theory:

$$\mathcal{L}_{\text{eff}} = \mathcal{L}_{\text{SM}} + \sum_i \frac{c_i^{(d)}}{\Lambda^{(d-4)}} O_i^{(d)} \tag{2.1}$$

Based on naturalness principle, bounds on $\Lambda$ can be derived assuming an effective coupling $c_i \approx 1$; alternatively, bounds on the respective couplings can be determined assuming that $\Lambda \approx \mathcal{O}(1)$ TeV. This approach allows useful and unified interpretation of many experimental results to derive stringent constraints on extensions of the SM in terms of few parameters (the coefficients of the higher-dimensional operators).

For instance, in a generic non-SM physics model, where suppression of FCNC processes is due only to the large masses of the particles that mediate them, i.e., the couplings are of order one, bounds on the scale $\Lambda$ that are compatible with the measurements of FCNC decay rates are determined. Depending on the process under study, this approach yields bounds of order $\Lambda \gtrsim 10^2$ TeV. Hence, either non-SM degrees of freedom emerge at energies higher than the TeV scale, or any SM extention at TeV scale must have a highly non-generic flavor structure, i.e., the coupling $c_i$ should have very suppressed values. Table 2.1 lists the bounds derived from measurements related to the mixing of neutral mesons for a choice of operators that change the flavor of the decaying quark by two unit in Eq. (2.1), showing the predictive power of this indirect approach in establishing general features of the theory (either its energy scale or its flavor structure), which hold independently of the dynamical details of the model.

The phenomenology of the $B$, $D$, and $K$ mesons is particularly useful for this purpose [10]. This thesis presents the analysis of the $B_s^0 \to J/\psi\phi$ decay, which

**Table 2.1** Bounds from experimental constraints on meson-mixing [8]

| Bounds on $\Lambda$ (TeV) | Bounds on $c_i$ ($\Lambda = 1$ TeV) | Mesons |
|---|---|---|
| $10^2$–$10^5$ | $10^{-11}$–$10^{-7}$ | $K^0 - \bar{K}^0$ |
| $10^3$–$10^4$ | $10^{-7}$–$10^{-8}$ | $D^0 - \bar{D}^0$ |
| $10^2$–$10^3$ | $10^{-7}$–$10^{-6}$ | $B^0 - \bar{B}^0$ |
| $10^2$–$10^3$ | $10^{-5}$ | $B_s^0 - \bar{B}_s^0$ |

allows a measurement of the $B_s^0 - \bar{B}_s^0$ mixing phase, an extremely powerful and still largely unconstrained experimental probe for a large class of non-SM physics phenomena.

## 2.3 CKM Matrix and *CP*-violation

In the SM the only source of flavor-changing interactions is originated from a rotation of the quarks flavor basis with respect to the weak-interaction basis in the Yukawa sector. Such rotation is given by a unitary $3 \times 3$ complex matrix,

$$V_{\text{CKM}} = \begin{pmatrix} V_{ud} & V_{us} & V_{ub} \\ V_{cd} & V_{cs} & V_{cb} \\ V_{td} & V_{ts} & V_{tb} \end{pmatrix},$$

known as the Cabibbo-Kobayashi-Maskawa (CKM) quark-mixing matrix [17, 18]. The constraints of unitarity of the CKM-matrix on the diagonal terms implies that the sum of all couplings of any of the up-type quarks to all the down-type quarks is the same for all generations, named *weak universality*, and derives from all $SU(2)$ doublets coupling with same strength to the vector bosons of weak interactions. Thus FCCC occurs at tree-level, while FCNC are mediated only by loops. A unitary $n \times n$ matrix contains $n^2$ independent real parameters, $2n-1$ of those can be eliminated by rephasing the $n$ up-type and $n$ down-type fermion fields (changing all fermions by the same phase obviously does not affect $V_{\text{CKM}}$); hence, there are $(n-1)^2$ physical parameters left. A unitary matrix is also orthogonal, and as such it contains $n(n-1)/2$ parameters corresponding to the independent rotation angles between the $n$ basis vectors; thus the remaining $(n-1)(n-2)/2$ parameters must be complex phases. For $n = 2$, i.e. two families, only one mixing angle remains, the Cabibbo angle and, no complex phases [17]. For $n = 3$ there are four physical parameters, namely three Euler angles and one irriducible phase, which provides a gateway for *CP* violation. The unitarity of the CKM matrix, $V_{\text{CKM}} V_{\text{CKM}}^{\dagger} = 1$, leads to 9 equations,

$$\sum_{k \in \{u,c,t\}} V_{ki} V_{kj}^{\star} = \delta_{ij} \qquad (i, j \in \{d, s, b\}).$$

Six require the sum of three complex quantities to vanish, and define triangles in the complex plane. The area of each triangle equals $J_{CP}/2$. The symbol $J_{CP}$ identifies the Jarlskog invariant [19], whose size quantifies the magnitude of violation of *CP* symmetry in the SM. The *CP* symmetry is violated only if $J_{CP} \neq 0$, as confirmed by current measurements [10]: $J_{CP} = (2.884^{+0.253}_{-0.053})10^{-5}$. Any *CP*-violating quantity in the SM is proportional to $J_{CP}$, reflecting the fact that a single complex phase appears in the $3 \times 3$ CKM matrix. This feature makes the SM implementation of *CP* violation

predictive, because all possible *CP* asymmetry measurements are correlated by their common origin from a single parameter of the theory.

The current knowledge of the CKM matrix elements magnitudes assuming unitarity is as follows [10]:

$$|V_{\rm CKM}| = \begin{pmatrix} 0.97426^{+0.00022}_{-0.00014} & 0.22539^{+0.00062}_{-0.00095} & 0.003501^{+0.000196}_{-0.000087} \\ 0.22526^{+0.00062}_{-0.00095} & 0.97345^{+0.00022}_{-0.00018} & 0.04070^{+0.00116}_{-0.00059} \\ 0.00846^{+0.00043}_{-0.00015} & 0.03996^{+0.00114}_{-0.00062} & 0.999165^{+0.000024}_{-0.000048} \end{pmatrix}. \tag{2.2}$$

The observed hierarchy $|V_{ub}| \ll |V_{cb}| \ll |V_{us}|$, and $|V_{cd}| \ll 1$, suggests an expansion in powers of $\lambda = |V_{us}| \approx 0.23$, the sine of the Cabibbo angle [20, 21]

$$V_{\rm CKM} = \begin{pmatrix} 1-\lambda^2/2-\lambda^4/8 & \lambda & A\lambda^3(\rho-i\eta) \\ -\lambda + A^2\lambda^5[1-2(\rho+i\eta)]/2 & 1-\lambda^2/2-\lambda^4(1+4A^2)/8 & A\lambda^2 \\ A\lambda^3[1-(1-\lambda^2/2)(\rho+i\eta)] & -A\lambda^2 + A\lambda^4[1-2(\rho+i\eta)]/2 & 1-A^2\lambda^4/2 \end{pmatrix} + \mathcal{O}(\lambda^6), \tag{2.3}$$

where $A \approx 0.80$, $\rho \approx 0.14$ and $\eta \approx 0.34$ are real parameters [10].

One triangular equation of particular phenomenological interest is referred to as the unitarity triangle (UT), because all three terms are roughly of the same size,

$$V_{ud}V_{ub}^\star + V_{cd}V_{cb}^\star + V_{td}V_{tb}^\star = 0; \tag{2.4}$$

The UT equation is normalized as

$$R_t e^{-i\beta} + R_u e^{i\gamma} = 1, \tag{2.5}$$

where

$$R_t = \left|\frac{V_{td}V_{tb}^\star}{V_{cd}V_{cb}^\star}\right|, \quad R_u = \left|\frac{V_{ud}V_{ub}^\star}{V_{cd}V_{cb}^\star}\right|, \quad \beta = \arg\left(-\frac{V_{cd}V_{cb}^\star}{V_{td}V_{tb}^\star}\right), \quad \gamma = \arg\left(-\frac{V_{ud}V_{ub}^\star}{V_{cd}V_{cb}^\star}\right), \tag{2.6}$$

are, respectively, two sides and two angles of the UT. The third side is the unit vector, and the third angle is $\alpha = \pi - \beta - \gamma = \arg[-V_{td}V_{tb}^\star / V_{ud}V_{ub}^\star]$. Equation (2.5) shows that all the information related to the UT is encoded in one complex number,

$$\bar\rho + i\bar\eta = R_u e^{i\gamma}, \tag{2.7}$$

which corresponds to the coordinates $(\bar\rho, \bar\eta)$ of the only nontrivial apex of the UT in the complex plane. Assuming that flavor-changing processes are fully described by the SM, the consistency of the various measurements with this assumption can be verified. The values of $\lambda$ and $A$ are known accurately from $K \to \pi l\nu$ and $b \to cl\nu$ decays respectively [7] to be

$$\lambda = 0.2257 \pm 0.0010, \quad A = 0.814 \pm 0.022. \tag{2.8}$$

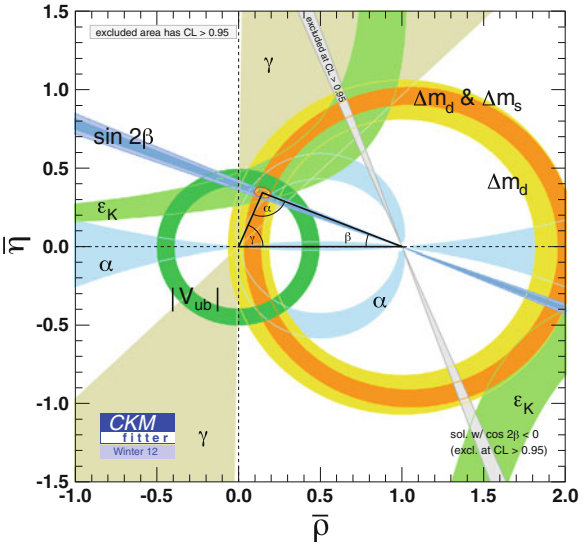


**Fig. 2.2** Constraints in the $(\bar{\rho}, \bar{\eta})$ plane. The *red hashed region* of the global combination corresponds to 68 % CL

All the relevant observables are then expressed as a function of the two remaining parameters $\bar{\rho}$ and $\bar{\eta}$, and checks are performed on whether there exists a range in the $(\bar{\rho}, \bar{\eta})$ plane that is consistent with all measurements. The resulting constraints in the $(\bar{\rho}, \bar{\eta})$ plane are shown in Fig. 2.2. The overall consistency is impressive, yielding the following values for $\bar{\rho}$ and $\bar{\eta}$ [7]:

$$\bar{\rho} = +0.135^{+0.031}_{-0.016}, \quad \bar{\eta} = +0.349 \pm 0.017. \tag{2.9}$$

This support the ansatz that flavor and *CP* violation in flavor-changing processes are dominated by the CKM mechanism. Such remarkable success of the SM suggests that arbitrary non-SM physics contributions in flavor-changing processes that occurs at tree-level are highly suppressed with respect to SM contributions [8].

A greater chance for detecting the effects of non-SM physics might reside in the study of loop-mediated FCNC transitions, such as the ones that mediates neutral-mesons oscillations described in Sect. 2.3.1.

### 2.3.1 $B_s^0$ Oscillations

Because of flavor mixing, flavored neutral mesons are subject to particle-antiparticle oscillations through weak transitions that change the flavor by two units, $\Delta F = 2$. The $\Delta B = 2$ FCNC quark transition that drives the $B_s^0 - \bar{B}_s^0$ oscillations is depicted

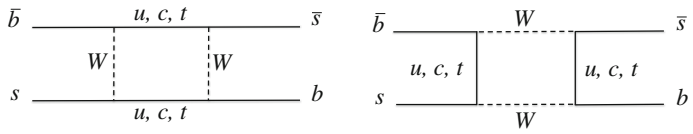


**Fig. 2.3** Feynman diagrams of transitions associated with $B_s^0 - \bar{B}_s^0$ oscillations

in Feynman diagrams of Fig. 2.3, called *box* diagrams. As a result of flavor mixing, a pure $B_s^0$ or $\bar{B}_s^0$ state at time $t = 0$, such as the meson states created from $p\bar{p} \to b\bar{b}$ interactions at the Tevatron, evolves to be a superposition of $B_s^0$ and $\bar{B}_s^0$ at time $t$:

$$|\psi(t)\rangle = a(t)|B_s^0\rangle + b(t)|\bar{B}_s^0\rangle. \tag{2.10}$$

In the Wigner-Weisskopf approximation, which neglects corrections to the exponential decay rate at very low or very high times, the effective Hamiltonian of the system can be written as

$$\mathbf{H_q} = \begin{pmatrix} M_{11}^s & M_{12}^s \\ M_{12}^{s*} & M_{22}^s \end{pmatrix} - \frac{i}{2}\begin{pmatrix} \Gamma_{11}^s & \Gamma_{12}^s \\ \Gamma_{12}^{s*} & \Gamma_{22}^s \end{pmatrix}, \tag{2.11}$$

where $M_{11}^s = M_{22}^s$ and $\Gamma_{11}^s = \Gamma_{22}^s$ hold under the assumption of *CPT* invariance which is a fairly general assumption thus far confirmed by any experimental verification [7]. The off-diagonal elements $M_{12}^s$ and $\Gamma_{12}^s$ are responsible for $B_s^0$–$\bar{B}_s^0$ mixing phenomena. The *dispersive* part $M_{12}^s$ corresponds to virtual $\Delta B = 2$ transitions dominated by heavy internal particles (top quarks in the SM) while the *absorptive* part $\Gamma_{12}^s$ arises from on-shell transitions due to decay modes common to $B_s^0$ and $\bar{B}_s^0$ mesons. Diagonalization of the Hamiltonian leads to two mass eigenstates $B_{\mathrm{H,L}}^s$ (H and L denote heavy and light, respectively), with mass $M_{\mathrm{H,L}}^s$ and decay width $\Gamma_{\mathrm{H,L}}^s$. The mass eigenstates are linear combinations of flavor eigenstates with complex coefficients $p$ and $q$ that satisfy $|p|^2 + |q|^2 = 1$,

$$|B_{\mathrm{L,H}}^s\rangle = p|B_s^0\rangle \pm q|\bar{B}_s^0\rangle\,. \tag{2.12}$$

The time evolution of the mass eigenstates is governed by the two eigenvalues, $m_H - \frac{i}{2}\Gamma_H$ and $m_L - \frac{i}{2}\Gamma_L$,

$$|B_{\mathrm{H,L}}^s(t)\rangle = e^{-i(m_{H,L}+i\Gamma_{H,L}/2)t}|B_{\mathrm{H,L}}^s(0)\rangle. \tag{2.13}$$

The time evolution of $B_s^0$ and $\bar{B}_s^0$ is derived from Eq. (2.13) and their definition in Eq. (2.12),

$$|B_s^0(t)\rangle = g_+(t)|B_s^0\rangle + \frac{q}{p}g_-(t)|\bar{B}_s^0\rangle,$$
$$|\bar{B}_s^0(t)\rangle = g_+(t)|\bar{B}_s^0\rangle + \frac{p}{q}g_-(t)|B_s^0\rangle, \tag{2.14}$$

where

$$g_+(t) = e^{-imt-\frac{\Gamma}{2}t}\left[\cosh\frac{\Delta\Gamma t}{4}\cos\frac{\Delta mt}{2} - i\sinh\frac{\Delta\Gamma t}{4}\sin\frac{\Delta mt}{2}\right],$$
$$g_-(t) = e^{-imt-\frac{\Gamma}{2}t}\left[-\sinh\frac{\Delta\Gamma t}{4}\cos\frac{\Delta mt}{2} + i\cosh\frac{\Delta\Gamma t}{4}\sin\frac{\Delta mt}{2}\right], \tag{2.15}$$

which satisfy

$$|g_\pm(t)|^2 = \frac{e^{-\Gamma t}}{2}\left[\cosh\frac{\Delta\Gamma t}{2} \pm \cos\Delta mt\right],$$
$$g_+^\star(t)g_-(t) = -\frac{e^{-\Gamma t}}{2}\left[\sinh\frac{\Delta\Gamma t}{2} + i\sin\Delta mt\right], \tag{2.16}$$

where $m = (m_H+m_L)/2, \Gamma = (\Gamma_H+\Gamma_L)/2, \Delta m = m_H - m_L$ and $\Delta\Gamma = \Gamma_L - \Gamma_H$.

The probabilities of observing a $B_s^0$ at any time $t$ if the meson was produced as either a $B_s^0$ or a $\bar{B}_s^0$ at $t = 0$ are

$$\begin{aligned}\mathcal{P}(B_s^0 \to B_s^0) &= |\langle B_s^0(t)|B_s^0(0)\rangle|^2 \\ &= |g_+(t)|^2 = \frac{e^{-\Gamma t}}{2}\left[\cosh\frac{\Delta\Gamma t}{2} + \cos\Delta mt\right], \\ \mathcal{P}(\bar{B}_s^0 \to B_s^0) &= |\langle B_s^0(t)|\bar{B}_s^0(0)\rangle|^2 \\ &= \left|\frac{p}{q}\right|^2|g_-(t)|^2 = \left|\frac{p}{q}\right|^2\frac{e^{-\Gamma t}}{2}\left[\cosh\frac{\Delta\Gamma t}{2} - \cos\Delta mt\right].\end{aligned} \tag{2.17}$$

The values of $M_{12}^s$ and $\Gamma_{12}^s$ are physical observables and can be determined from measurements of the following quantities (for more details see, e.g., Ref. [22]):

- the mass difference between the heavy and light mass eigenstates

$$\Delta m_s \equiv m_{\rm H}^s - m_{\rm L}^s \approx 2|M_{12}^s|\left(1 - \frac{|\Gamma_{12}^s|^2}{8|M_{12}^s|^2}\sin^2\phi_{12}^s\right), \tag{2.18}$$

  where $\phi_{12}^s = \arg(-M_{12}^s/\Gamma_{12}^s)$ is convention-independent;
- the decay width difference between the light and heavy mass eigenstates

$$\Delta\Gamma_s \equiv \Gamma_{\rm L}^s - \Gamma_{\rm H}^s \approx 2|\Gamma_{12}^s|\cos\phi_{12}^s\left(1 + \frac{|\Gamma_{12}^s|^2}{8|M_{12}^s|^2}\sin^2\phi_{12}^s\right); \tag{2.19}$$

- the flavor-specific asymmetry

$$a_{\mathrm{sl}}^{s} \equiv \frac{|p/q|^2 - |q/p|^2}{|p/q|^2 + |q/p|^2} \approx \frac{|\Gamma_{12}^{s}|}{|M_{12}^{s}|} \sin\phi_{12}^{s} \approx \frac{\Delta\Gamma_s}{\Delta m_s} \tan\phi_{12}^{s} \,. \tag{2.20}$$

The correction terms proportional to $\sin^2\phi_{12}^{s}$ in Eqs. (2.18) and (2.19) are irrelevant compared to the present size of experimental uncertainties. In addition, the ratio of $q$ and $p$ can be expressed as

$$\left(\frac{q}{p}\right) = -\frac{\Delta m_s + \frac{i}{2}\Delta\Gamma_s}{2(M_{12}^{s} - \frac{i}{2}\Gamma_{12}^{s})}. \tag{2.21}$$

The possibility of flavor oscillations strongly enriches the phenomenology of *CP* violation, which occurs in $B_s^0$ meson decays through three different manifestations. Considering a decay in a *CP* eigenstate $f$ with eigenvalue $\eta_f$ and $A_f$ being the decay amplitude of $B_s^0 \to f$, we define the following classes of *CP* violation:

- *CP violation in decay* or *direct CP violation*, which is the only possible *CP* violating effect in charged meson decays since they cannot undergo mixing, occurs when the amplitude of decay to a final state is not the same as the amplitude of the *CP* conjugate of the initial state decaying to the *CP* conjugate of the final state, $|\bar{A}_{\bar{f}}|/|A_f| \neq 1$. In the $B_s^0 \to J/\psi\phi$ channel, the standard model *CP*-violating weak phase in the decay is suppressed by a factor of $\lambda^2$ [23]. Hence, the assumption of no direct *CP* violation in $B_s^0 \to J/\psi\phi$ decays, $|\bar{A}_{\bar{f}}| = |A_f|$, holds to a very good approximation.
- *CP violation in mixing* occurs when $|q/p| \neq 1$. In the $B_s^0$ meson system, the CKM model predicts $|q/p| = 1 + \mathcal{O}(10^{-3})$ [24]. In semileptonic $B_s^0$ decays this leads to a charge asymmetry in the decay products, but in $B_s^0 \to J/\psi\phi$ the factor $|q/p|$ is not isolated, therefore *CP* violation in mixing is not directly measured in this analysis.
- *CP violation due to interference between decays with and without mixing* may appear in the evolution of $B_s^0$ and $\bar{B}_s^0$ mesons decay. This type of *CP* violation is observable by measuring the phase difference between the amplitude for a direct decay to a final state $f$ and the amplitude for a decay produced by oscillation, discussed in the next section.

## 2.4 Analysis of the Time-Evolution of $B_s^0 \to J/\psi\phi$ Decays

For decays dominated by the $b \to c\bar{c}s$ tree amplitude, the phase difference is denoted by

$$\phi_s \equiv -\arg\left(\eta_f \frac{q}{p} \frac{\bar{A}_f}{A_f}\right), \tag{2.22}$$

where $A_f$ and $\bar{A}_f$ are the decay amplitudes of $B_s^0 \to f$ and $\bar{B}_s^0 \to f$, respectively. In the absence of direct *CP* violation $\bar{A}_f/A_f = \eta_f$. With these approximations, the *CP* violating phases appearing in $B_s^0$ mixing reduce to the phase $\phi_s \approx -2\beta_s^{J/\psi\phi}$, defined as [25]

$$\beta_s^{J/\psi\phi} \equiv \arg\left(-\frac{V_{ts}V_{tb}^*}{V_{cs}V_{cb}^*}\right). \tag{2.23}$$

If non-SM physics occurs in $M_{12}^s$ or in the decay amplitudes, the measured value of $\beta_s^{J/\psi\phi}$ can differ from the true value of $\beta_s^{\mathrm{SM}}$:

$$2\beta_s^{J/\psi\phi} = 2\beta_s^{\mathrm{SM}} - \phi_s^{\mathrm{NP}} \tag{2.24}$$

where from the experimental constraints on the CKM-matrix elements [26], $-2\beta_s^{\mathrm{SM}}$ assumes the value

$$2\beta_s^{\mathrm{SM}} = 0.0363^{+0.0016}_{-0.0015}. \tag{2.25}$$

With the current experimental sensitivity, the non-SM physics phase would be expected to dominate a measurement of phase. The study of the time evolution of $B_s^0 \to J/\psi\phi$ decays is widely recognized as the best way to probe *CP*-violation in the interefence between mixing and decay in the $B_s^0$ sector. The $J/\psi\phi$ final state is common to $B_s^0$ and $\bar{B}_s^0$ decays, a necessary condition for mixing-induced *CP* violation to occur. The mixing phase becomes observable through the interference of two amplitudes, the amplitude of direct decay and the amplitude of decay preceded by mixing to a common final-state, Fig. 2.4. What is actually observable is the phase *difference* between decay and mixing, but since the decay is dominated by a single real amplitude, the difference approximates accurately the mixing phase. The fact that the decay is strongly dominated by a single, tree-level, real amplitude is what makes the extraction of the mixing phase from this process theoretically solid. Subleading *penguin* amplitudes are expected to contribuite at the $\mathcal{O}(10^{-3})$ level [27–29], introducing additional phases that in principle complicate the theoretical interpretation of the experimental results. While these effects are completely negligible compared to the expected resolution of the present measurement, they will likely need to be accounted for in the interpretation of future, more precise results.

Because of the spin-composition of the initial- and final-state particles, angular momentum conservation imposes a relative angular momentum ($L$) between the

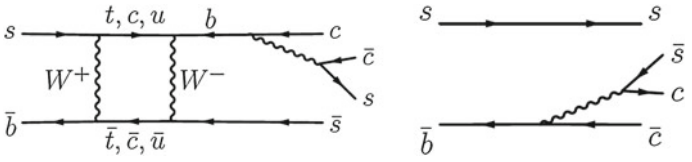


**Fig. 2.4** Leading Feynman graph of the $B_s^0 \to J/\psi\phi$ decay with (*left*) and without (*right*) mixing

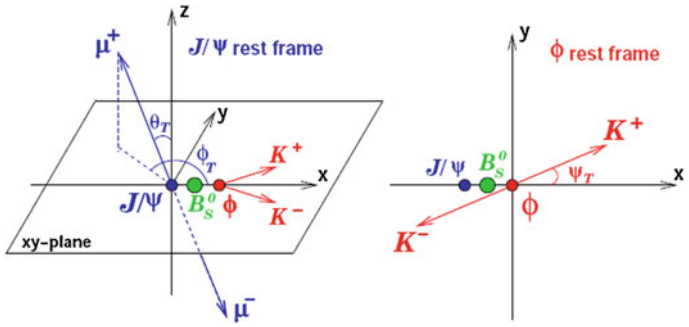


**Fig. 2.5** Graphical rappresentation of the relevant angles in the transversity basis

vector (spin-1) final-state particles in order to match the zero net total angular momentum of the initial state. Three independent decay amplitudes determine the transition probability, each corresponding to one of the three possible relative angular momenta, $L = 0, 1, 2$. The transversity basis illustrated in Fig. 2.5, is particularly convenient because when applied to the amplitude, it allows to separate the latter into three terms, each corresponding to a definite $CP$ eigenvalue of the final state, and their interferences. Determining independently the time evolution of decays into $CP$-even and $CP$-odd final states enhances the sensitivity to the $CP$-violating phase, while providing also access to observables, arising from the interference between components with opposite $CP$ parity, that do not vanish even if the evolution of initially produced $B_s^0$ and $\bar{B}_s^0$ mesons are not separated with flavor-tagging. A candidate-specific determination of the $CP$ parity is not possible, but angular distributions of final-state particles are used to statistically separate $CP$-even and $CP$-odd components. Three angles completely define the kinematic distributions of the four final-state particles. In the transversity basis the angles are defined in two different frames. In the following, $\overrightarrow{p}\,(A)_B$ denotes the three momentum of particle $A$ in the rest frame of particle $B$. The angle $\Psi$ of the $K^+$ is defined in the $\phi$ rest frame as the angle between $\overrightarrow{p}\,(K^+)$ and the negative $J/\psi$ direction:

$$\cos\Psi = -\frac{\overrightarrow{p}\,(K^+)_\phi \cdot \overrightarrow{p}\,(J/\psi)_\phi}{|\overrightarrow{p}\,(K^+)_\phi| \cdot |\overrightarrow{p}\,(J/\psi)_\phi|}. \tag{2.26}$$

To calculate the other two angles, we first define a coordinate system through the directions

$$\hat{x} = \frac{\overrightarrow{p}\,(\phi)_{J/\psi}}{|\overrightarrow{p}\,(\phi)_{J/\psi}|}, \quad \hat{y} = \frac{\overrightarrow{p}\,(K^+)_{J/\psi} - [\overrightarrow{p}\,(K^+)_{J/\psi} \cdot \hat{x}]\hat{x}}{|\overrightarrow{p}\,(K^+)_{J/\psi} - [\overrightarrow{p}\,(K^+)_{J/\psi} \cdot \hat{x}]\hat{x}|}, \quad \hat{z} = \hat{x} \times \hat{y}. \tag{2.27}$$

The following angles of the direction of the $\mu^+$ in the $J/\psi$ rest frame are calculated as

$$\cos\Theta = \frac{\overrightarrow{p}\,(\mu^+)_{J/\psi}}{|\overrightarrow{p}\,(\mu^+)_{J/\psi}|}\cdot\hat{z}, \quad \Phi = \arctan\left(\frac{\frac{\overrightarrow{p}\,(\mu^+)_{J/\psi}}{|\overrightarrow{p}\,(\mu^+)_{J/\psi}|}\cdot\hat{y}}{\frac{\overrightarrow{p}\,(\mu^+)_{J/\psi}}{|\overrightarrow{p}\,(\mu^+)_{J/\psi}|}\cdot\hat{x}}\right) \tag{2.28}$$

where the ambiguity of the angle $\Phi$ is lifted by using the signs of the $\overrightarrow{p}\,(\mu^+)_{J/\psi}\cdot\hat{x}$ and $\overrightarrow{p}\,(\mu^+)_{J/\psi}\cdot\hat{y}$ dot products.

The decay is further described in terms of the polarization states of the vector mesons, either longitudinal (0), or transverse to their directions of motion, and in the latter case, parallel ($||$) or perpendicular ($\perp$) to each other. The corresponding amplitudes, which depend on time $t$, are $A_0$, $A_{||}$ and $A_\perp$, respectively. The transverse linear polarization amplitudes $A_{||}$ and $A_\perp$ correspond to $CP$-even and $CP$-odd final states at decay time $t = 0$, respectively. The longitudinal polarization amplitude $A_0$ corresponds to a $CP$-even final state. The angular distribution of $B_s^0 \to J/\phi(\to \mu^+\mu^-)\phi(\to K^+K^-)$ decays reads,

$$\frac{1}{\overset{(-)}{\Gamma}}\frac{\mathrm{d}^3\overset{(-)}{\Gamma}(\overset{(-)}{B}{}^0_s \to J/\psi\phi)}{\mathrm{d}\cos\Theta\,\mathrm{d}\Phi\,\mathrm{d}\cos\Psi} = \frac{\sum_{i=1}^{6}\left[\overset{(-)}{K}{}_i\, f_i(\cos\Theta,\Phi,\cos\Psi)\right]}{|\overset{(-)}{A}{}_0|^2 + |\overset{(-)}{A}{}_{||}|^2 + |\overset{(-)}{A}{}_\perp|^2}, \tag{2.29}$$

with the $K_i$ and $f_i(\cos\Theta,\Phi,\cos\Psi)$ terms detailed in Table 2.2. Figure 2.6 shows some examples of transversity-angles distributions in $B_s^0 \to J/\psi\phi$ decays for three sets of polarization amplitudes, illustrating how the distribution of these observables depend on the underlying physics parameters.

Effects from $B_s^0 - \bar{B}_s^0$ oscillations are introduced along with the decay transition to the final state. The time evolution is independent of the angular distributions, and it is encoded through a time-dependence of the polarization amplitudes, i.e., the $K_i$ terms of Eq. (2.29):

$$K_i \to K_i(t),$$

**Table 2.2** Angular functions in terms of transversity angles and corresponding transversity amplitudes for the $B_s^0 \to J/\psi\phi$ decay entering Eq. (2.29)

| i | $\overset{(-)}{K}{}_i$ | $f_i(\cos\Theta,\Phi,\cos\Psi)$ |
|---|---|---|
| 1 | $\lvert\overset{(-)}{A}{}_0\rvert^2$ | $\frac{9}{32\pi}2\cos^2\Psi(1-\sin^2\Theta\cos^2\Phi)$ |
| 2 | $\lvert\overset{(-)}{A}{}_{\|\|}\rvert^2$ | $\frac{9}{32\pi}\sin^2\Psi(1-\sin^2\Theta\sin^2\Phi)$ |
| 3 | $\lvert\overset{(-)}{A}{}_\perp\rvert^2$ | $\frac{9}{32\pi}\sin^2\Psi\sin^2\Theta$ |
| 4 | $\mathfrak{Im}(\overset{(-)}{A}{}_\perp\overset{(-)}{A}{}^\star_{\|\|})$ | $-\frac{9}{32\pi}\sin^2\Psi\sin 2\Theta\sin\Phi$ |
| 5 | $\mathfrak{Re}(\overset{(-)}{A}{}_{\|\|}\overset{(-)}{A}{}^\star_0)$ | $\frac{9}{32\pi}\frac{\sqrt{2}}{2}\sin 2\Psi\sin^2\Theta\sin 2\Phi$ |
| 6 | $\mathfrak{Im}(\overset{(-)}{A}{}_\perp\overset{(-)}{A}{}^\star_0)$ | $\frac{9}{32\pi}\frac{\sqrt{2}}{2}\sin 2\Psi\sin 2\Theta\cos\Phi$ |

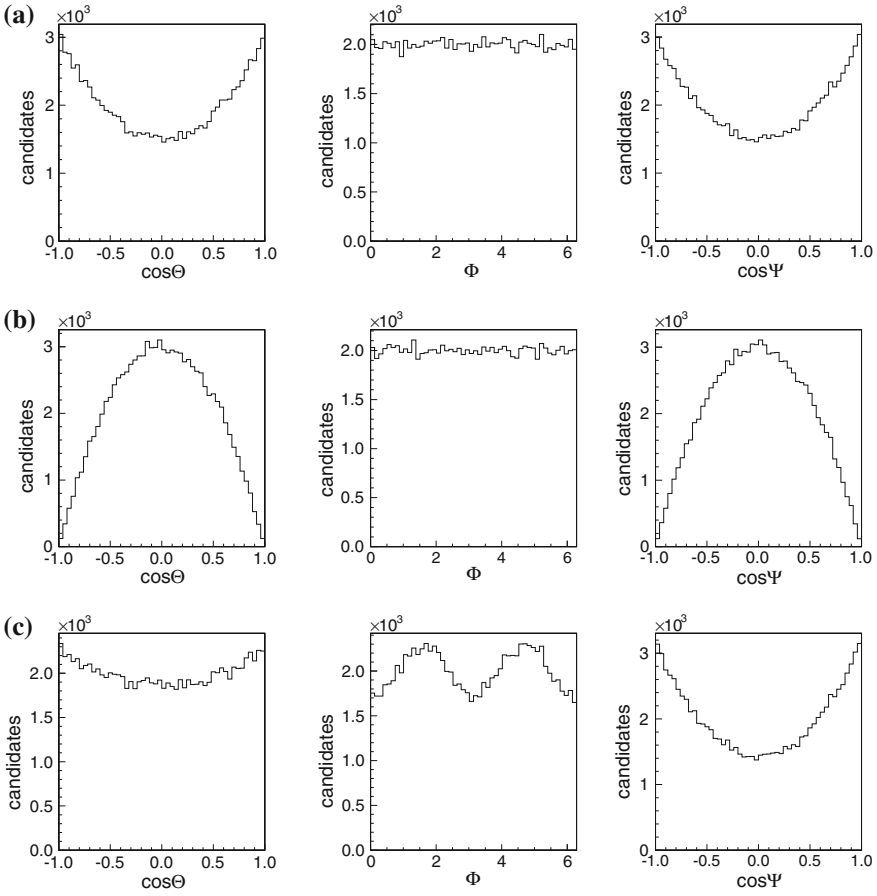


**Fig. 2.6** Example of transversity angles distributions. In **a** the $CP$-odd amplitude $A_\perp$ is set zero, while both $|A_0|^2$ and $|A_\parallel|^2$ are set to 50 %. In **b** the $CP$-even amplitudes $A_0$ and $A_\perp$ are set to zero. In **c** the amplitudes and strong phases are set to the value measured in Ref. [30]: $|A_0|^2 = 0.524$, $|A_\parallel|^2 = 0.231$, $\delta_\perp = 2.95$, and we take $\delta_\parallel = \pi$. Note that the angle $\Phi$ has a non-uniform distribution if there is an interference between the $CP$-even and $CP$-odd amplitudes

where $t$ is the decay-time. By using Eqs. (2.14) and (2.16) and considering the $CP$ parity of each transversity amplitude, one can derive the time development for each $K_i(t)$ term. The decay rate of an initially produced $\overset{(-)}{B}{}^0_s$ meson is written as a function of the decay time and transversity angles as in Ref. [31]. In Table 2.3, we list the $\overset{(-)}{K}{}_i(t)$ terms, where the polarization amplitudes at $t = 0$ for an initially produced $\overset{(-)}{B}{}^0_s$ meson are defined as

**Table 2.3** General expressions of $K_i(t)$ ($\bar{K}_i(t)$) terms for $B_s^0 \to J/\psi\phi$ decays, where both direct and interference *CP* violation are allowed

| i | $\overset{(-)}{K}_i$ |
|---|---|
| 1 | $\frac{1}{2}e^{-\Gamma t}\Big[\big(\lvert A_0\rvert^2+\lvert\bar{A}_0\rvert^2\big)\cosh(\Delta\Gamma_s t/2) \overset{(-)}{+} \big(\lvert A_0\rvert^2-\lvert\bar{A}_0\rvert^2\big)\cos\Delta m_s t$ $-2\Re\mathrm{e}(A_0^\star\bar{A}_0)\Big(\cos 2\phi_M^s \sinh(\Delta\Gamma_s t/2) \overset{(+)}{-} \sin 2\phi_M^s \sin\Delta m_s t\Big)$ $-2\Im\mathrm{m}(A_0^\star\bar{A}_0)\Big(\overset{(-)}{+}\cos 2\phi_M^s \sin\Delta m_s t+\sin 2\phi_M^s \sinh(\Delta\Gamma_s t/2)\Big)\Big]$ |
| 2 | $\frac{1}{2}e^{-\Gamma t}\Big[\big(\lvert A_\parallel\rvert^2+\lvert\bar{A}_\parallel\rvert^2\big)\cosh(\Delta\Gamma_s t/2) \overset{(-)}{+} \big(\lvert A_\parallel\rvert^2-\lvert\bar{A}_\parallel\rvert^2\big)\cos\Delta m_s t$ $-2\Re\mathrm{e}(A_\parallel^\star\bar{A}_\parallel)\Big(\cos 2\phi_M^s \sinh(\Delta\Gamma_s t/2) \overset{(+)}{-} \sin 2\phi_M^s \sin\Delta m_s t\Big)$ $-2\Im\mathrm{m}(A_\parallel^\star\bar{A}_\parallel)\Big(\overset{(-)}{+}\cos 2\phi_M^s \sin\Delta m_s t+\sin 2\phi_M^s \sinh(\Delta\Gamma_s t/2)\Big)\Big]$ |
| 3 | $\frac{1}{2}e^{-\Gamma t}\Big[\big(\lvert A_\perp\rvert^2+\lvert\bar{A}_\perp\rvert^2\big)\cosh(\Delta\Gamma_s t/2) \overset{(-)}{+} \big(\lvert A_\perp\rvert^2-\lvert\bar{A}_\perp\rvert^2\big)\cos\Delta m_s t$ $+2\Re\mathrm{e}(A_\perp^\star\bar{A}_\perp)\Big(\cos 2\phi_M^s \sinh(\Delta\Gamma_s t/2) \overset{(+)}{-} \sin 2\phi_M^s \sin\Delta m_s t\Big)$ $+2\Im\mathrm{m}(A_\perp^\star\bar{A}_\perp)\Big(\overset{(-)}{+}\cos 2\phi_M^s \sin\Delta m_s t+\sin 2\phi_M^s \sinh(\Delta\Gamma_s t/2)\Big)\Big]$ |
| 4 | $\frac{1}{2}e^{-\Gamma t}\Big[\Im\mathrm{m}(A_\perp A_\parallel^\star-\bar{A}_\perp\bar{A}_\parallel^\star)\cosh(\Delta\Gamma_s t/2) \overset{(-)}{+} \Im\mathrm{m}(A_\perp A_\parallel^\star+\bar{A}_\perp\bar{A}_\parallel^\star)\cos\Delta m_s t$ $+\Im\mathrm{m}(A_\perp\bar{A}_\parallel^\star-\bar{A}_\perp A_\parallel^\star)\Big(-\sinh(\Delta\Gamma_s t/2)\cos 2\phi_M^s \overset{(-)}{+} \sin\Delta m_s t \sin 2\phi_M^s\Big)$ $+\Re\mathrm{e}(A_\perp\bar{A}_\parallel^\star+\bar{A}_\perp A_\parallel^\star)\Big(-\sinh(\Delta\Gamma_s t/2)\sin 2\phi_M^s \overset{(+)}{-} \sin\Delta m_s t\cos 2\phi_M^s\Big)\Big]$ |
| 5 | $\frac{1}{2}e^{-\Gamma t}\Big[\Re\mathrm{e}(A_\parallel A_0^\star+\bar{A}_\parallel\bar{A}_0^\star)\cosh(\Delta\Gamma_s t/2) \overset{(-)}{+} \Re\mathrm{e}(A_\parallel A_0^\star-\bar{A}_\parallel\bar{A}_0^\star)\cos\Delta m_s t$ $+\Re\mathrm{e}(A_\parallel\bar{A}_0^\star+\bar{A}_\parallel A_0^\star)\Big(-\sinh(\Delta\Gamma_s t/2)\cos 2\phi_M^s \overset{(-)}{+} \sin\Delta m_s t \sin 2\phi_M^s\Big)$ $+\Im\mathrm{m}(A_\parallel\bar{A}_0^\star-\bar{A}_\parallel A_0^\star)\Big(\sinh(\Delta\Gamma_s t/2)\sin 2\phi_M^s \overset{(-)}{+} \sin\Delta m_s t\cos 2\phi_M^s\Big)\Big]$ |
| 6 | $\frac{1}{2}e^{-\Gamma t}\Big[\Im\mathrm{m}(A_\perp A_0^\star-\bar{A}_\perp\bar{A}_0^\star)\cosh(\Delta\Gamma_s t/2) \overset{(-)}{+} \Im\mathrm{m}(A_\perp A_0^\star+\bar{A}_\perp\bar{A}_0^\star)\cos\Delta m_s t$ $+\Im\mathrm{m}(A_\perp\bar{A}_0^\star-\bar{A}_\perp A_0^\star)\Big(-\sinh(\Delta\Gamma_s t/2)\cos 2\phi_M^s \overset{(-)}{+} \sin\Delta m_s t \sin 2\phi_M^s\Big)$ $+\Re\mathrm{e}(A_\perp\bar{A}_0^\star+\bar{A}_\perp A_0^\star)\Big(-\sinh(\Delta\Gamma_s t/2)\sin 2\phi_M^s \overset{(+)}{-} \sin\Delta m_s t\cos 2\phi_M^s\Big)\Big]$ |

$$
\begin{aligned}
\overset{(-)}{A}_0(t=0) &= \overset{(-)}{A}_0 = \langle J/\psi\phi, 0 \mid \overset{(-)}{B_s^0}\rangle,\\
\overset{(-)}{A}_\parallel(t=0) &= \overset{(-)}{A}_\parallel = \langle J/\psi\phi, \parallel \mid \overset{(-)}{B_s^0}\rangle,\\
\overset{(-)}{A}_\perp(t=0) &= \overset{(-)}{A}_\perp = \langle J/\psi\phi, \perp \mid \overset{(-)}{B_s^0}\rangle,
\end{aligned}
\tag{2.30}
$$

The expressions in Table 2.3 refer to the most general case for the time evolution of a $B_s^0$-decay into a vector–vector and self-conjugate final state. By constructing the quantity

$$
\frac{K_i(t)-\bar{K}_i(t)}{K_i(t)+\bar{K}_i(t)} \tag{2.31}
$$

with $i = (1, 2, 3, 5)$, one can obtain the time-dependent *CP* asymmetry

$$\mathcal{A}_{CP}(t) = \frac{\Gamma(B_s^0 \to \bar{f}) - \Gamma(\bar{B}_s^0 \to f)}{\Gamma(B_s^0 \to \bar{f}) + \Gamma(\bar{B}_s^0 \to f)} \simeq \frac{\mathcal{C}_f \cos(\Delta m_s t) - \mathcal{S}_f \sin(\Delta m_s t)}{\cosh(\Delta\Gamma_s t/2) + \mathcal{S}'_f \sinh(\Delta\Gamma_s t/2)}. \tag{2.32}$$

where

$$\mathcal{C}_f = \frac{1 - |\lambda_f|^2}{1 + |\lambda_f|^2}, \quad \mathcal{S}_f = \frac{2\mathfrak{Im}(\lambda_f)}{1 + |\lambda_f|^2}, \quad \mathcal{S}'_f = \frac{2\mathfrak{Re}(\lambda_f)}{1 + |\lambda_f|^2}, \tag{2.33}$$

This includes both *direct* and *interference CP* violation.

In particular, the polarization amplitudes are written as follows:

$$\begin{aligned} \overset{(-)}{A}_0 &= |\overset{(-)}{A}_0| e^{\overset{(-)}{+} i\phi_{A_0}} e^{i\delta_0}, \\ \overset{(-)}{A}_\parallel &= |\overset{(-)}{A}_\parallel| e^{\overset{(-)}{+} i\phi_{A_\parallel}} e^{i\delta_\parallel}, \\ \overset{(-)}{A}_\perp &= |\overset{(-)}{A}_\perp| e^{\overset{(-)}{+} i\phi_{A_\perp}} e^{i\delta_\perp}, \end{aligned} \tag{2.34}$$

with $\phi_{A_i}$ and $\delta_i$ being the weak and strong phases of the amplitudes, respectively. Table 2.3 emphasizes the two distinct sources of *CP* violation. The terms proportional to $\mathfrak{Re}(\overset{(-)}{A}_i \overset{(-)}{A}_j{}^\star)$ and to $\mathfrak{Im}(\overset{(-)}{A}_i \overset{(-)}{A}_j{}^\star)$ in the $\overset{(-)}{K}_i(t)$ terms encode the dependence on both $\phi_{A_i}$ and $\delta_i$. The time-evolution functions $K_i(t)$ are reported in Table 2.4 in a compact form that emphasizes the equality of the time dependence for final states with the same *CP*-parity. We have defined

**Table 2.4** Expressions of $K_i(t)$ terms of the $B_s^0 \to J/\psi\phi$ decay rate, where only interference *CP* violation is allowed

| i | $\overset{(-)}{K}_i(t)$ | *CP* parity |
|---|---|---|
| 1 | $\lvert\overset{(-)}{A}_0\rvert^2 \overset{(-)}{\mathcal{O}}{}^+(t)$ | Even |
| 2 | $\lvert\overset{(-)}{A}_\parallel\rvert^2 \overset{(-)}{\mathcal{O}}{}^+(t)$ | Even |
| 3 | $\lvert\overset{(-)}{A}_\perp\rvert^2 \overset{(-)}{\mathcal{O}}{}^-(t)$ | Odd |
| 4 | $\lvert\overset{(-)}{A}_\parallel\rvert\lvert\overset{(-)}{A}_\perp\rvert \overset{(-)}{\mathcal{E}}_{\mathfrak{Im}}(t, \delta_\perp - \delta_\parallel)$ | Mix |
| 5 | $\lvert\overset{(-)}{A}_\parallel\rvert\lvert\overset{(-)}{A}_0\rvert \cos\delta_\parallel \overset{(-)}{\mathcal{O}}{}^+(t)$ | Even |
| 6 | $\lvert\overset{(-)}{A}_\perp\rvert\lvert\overset{(-)}{A}_0\rvert \overset{(-)}{\mathcal{E}}_{\mathfrak{Im}}(t, \delta_\perp)$ | Mix |

The third column reports the *CP* parity of each term. The formulae of $\mathcal{O}^\pm$ and $\mathcal{E}_{\mathfrak{Im}}$ are given by Eqs. (2.35) and (2.36), while the phases $\delta_\parallel$ and $\delta_\perp$ are defined by Eq. (2.37)

$$\overset{(-)}{\mathcal{O}}{}^{\pm}(t) = e^{-\Gamma t}\left(\cosh\frac{\Delta\Gamma_s t}{2} \mp \cos 2\beta_s^{J/\psi\phi}\sinh\frac{\Delta\Gamma_s t}{2} \overset{(\mp)}{\pm} \sin 2\beta_s^{J/\psi\phi}\sin\Delta m_s t\right), \tag{2.35}$$

$$\overset{(-)}{\mathcal{E}}{}_{\mathfrak{Im}}(t,\alpha) = e^{-\Gamma t}\left(\overset{(-)}{+}\sin\alpha\cos\Delta m_s t \overset{(+)}{-}\cos\alpha\cos 2\beta_s^{J/\psi\phi}\sin\Delta m_s t - \cos\alpha\sin 2\beta_s^{J/\psi\phi}\sinh\frac{\Delta\Gamma_s t}{2}\right). \tag{2.36}$$

The phase $\alpha$ in the above equations represents the *CP*-conserving phase associated with the polarization amplitudes. Since only phase differences matter, a customary convention is to choose $A_0$ real and define the strong phases of the transverse amplitudes as

$$\delta_\parallel = \arg\left(\frac{A_\parallel}{A_0}\right) = \arg\left(\frac{\bar{A}_\parallel}{\bar{A}_0}\right), \tag{2.37}$$
$$\delta_\perp = \arg\left(\frac{A_\perp}{A_0}\right) = \arg\left(\frac{\bar{A}_\perp}{\bar{A}_0}\right).$$

### 2.4.1 Time Evolution of the (S + P)-wave System

Thus far we only considered $K^+K^-$ pairs originated from the decay of $\phi(1020)$ mesons. However, the $K^+K^-$ final state could include a mixture of multiple resonances, their interference, and also contribution from non-resonant production. Neglecting the contamination of $s\bar{s}$-quark states of zero spin and mass close to the $\phi(1020)$ pole, such as the $f_0(980)$ [7], may induce a bias in the estimation of the *CP*-odd fraction of the signal and alter the measurement of $\beta_s^{J/\psi\phi}$ [32].

We now focus on the decay $B_s^0 \to J/\psi X(\to K^+K^-)$. The $f_0(980)$ is a spin-0 meson that may contribute and its contribution is called often *S-wave*, while the $\phi(1020)$ is a spin-1 meson and its contribution is denoted as *P-wave*. A fraction of $B_s^0 \to J/\psi K^+K^-$ decays may be present with a non-resonant $K^+K^-$ pair that has a relative angular momentum $L = 1$ with respect the $J/\psi$ state. Such contributions are expected to be significantly smaller than the resonant fraction, because their amplitude involves the production of an extra $u\bar{u}$-quark pair with respect to the amplitude for the resonances' production. Hence, the non-resonant component is not further considered. The partial-wave classification of the various contributions to the $K^+K^-$ spectrum, which is based on the spin of the resonance, should not be confused with the partial-wave basis of the polarization amplitudes, which is based on the value of the relative angular momentum between two resonances. In what follows, the partial-waves nomenclature is used only for referring to the $K^+K^-$

resonances spectrum, while for polarization amplitudes only the transversity basis is used.

The differential decay rates considered so far—e.g., Eq. (2.29)—are parametrized as functions of transversity angles and decay time. However, they also depend on the invariant $K^+K^-$ mass $m$, resulting in amplitudes that are functions of $m$ as well [33, 34]. To account for the total $S+P$ contribution in the decay rate, the $P$-wave amplitude and the $S$-wave amplitude are summed; then the total decay rate is decomposed as follows [33, 34]:

$$\begin{aligned}\frac{\mathrm{d}^5 \overset{(-)}{\Gamma}(\overset{(-)}{B}{}^0_s \to J/\psi K^+K^-)}{\mathrm{d}m\,\mathrm{d}t\,\mathrm{d}\cos\Theta\,\mathrm{d}\Phi\,\mathrm{d}\cos\Psi} &= |\overset{(-)}{P}{}_{\text{wave}} + \overset{(-)}{S}{}_{\text{wave}}|^2 \\ &= |\overset{(-)}{P}{}_{\text{wave}}|^2 + |\overset{(-)}{S}{}_{\text{wave}}|^2 + 2\,\mathfrak{Re}\left(\overset{(-)}{P}{}_{\text{wave}}\,\overset{(-)}{S}{}^{\star}_{\text{wave}}\right),\end{aligned} \tag{2.38}$$

Usually, in analyses of $B_s^0 \to J/\psi\phi$ decays, the dependence on $m$ is integrated out and the measurement of the polarization amplitudes is obtained from angular distributions only, obtaining

$$\frac{1}{\overset{(-)}{\Gamma}}\frac{\mathrm{d}^4\overset{(-)}{\Gamma}(\overset{(-)}{B}{}^0_s \to J/\psi K^+K^-)}{\mathrm{d}t\,\mathrm{d}\cos\Theta\,\mathrm{d}\Phi\,\mathrm{d}\cos\Psi} = \frac{\sum_{i=1}^{10}\left[\overset{(-)}{K}{}_i(t)\,f_i(\cos\Theta,\Phi,\cos\Psi)\right]}{|\overset{(-)}{A}{}_0|^2 + |\overset{(-)}{A}{}_\parallel|^2 + |\overset{(-)}{A}{}_\perp|^2 + |\overset{(-)}{A}{}_S|^2}, \tag{2.39}$$

**Table 2.5** Expressions of $K_i(t)$ ($\bar{K}_i(t)$) and $f_i(\cos\Theta,\Phi,\cos\Psi)$ terms of the $B_s^0 \to J/\psi K^+K^-$ decay rate, where the dependence on the mass $m$ is integrated out

| i | $\overset{(-)}{K}{}_i(t)$ | $f_i(\cos\Theta,\Phi,\cos\Psi)$ | $CP$ parity |
|---|---|---|---|
| 1 | $\lvert\overset{(-)}{A}{}_0\rvert^2\,\overset{(-)}{\mathcal{O}}{}^+(t)$ | $\frac{9}{32\pi}2\cos^2\Psi(1-\sin^2\Theta\cos^2\Phi)$ | Even |
| 2 | $\lvert\overset{(-)}{A}{}_\parallel\rvert^2\,\overset{(-)}{\mathcal{O}}{}^+(t)$ | $\frac{9}{32\pi}\sin^2\Psi(1-\sin^2\Theta\sin^2\Phi)$ | Even |
| 3 | $\lvert\overset{(-)}{A}{}_\perp\rvert^2\,\overset{(-)}{\mathcal{O}}{}^-(t)$ | $\frac{9}{32\pi}\sin^2\Psi\sin^2\Theta$ | Odd |
| 4 | $\lvert\overset{(-)}{A}{}_\parallel\rvert\lvert\overset{(-)}{A}{}_\perp\rvert\,\overset{(-)}{\mathcal{E}}{}_{\Im\mathrm{m}}(t,\delta_\perp-\delta_\parallel)$ | $-\frac{9}{32\pi}\sin^2\Psi\sin 2\Theta\sin\Phi$ | Mix |
| 5 | $\lvert\overset{(-)}{A}{}_\parallel\rvert\lvert\overset{(-)}{A}{}_0\rvert\cos\delta_\parallel\,\overset{(-)}{\mathcal{O}}{}^+(t)$ | $\frac{9}{32\pi}\frac{\sqrt{2}}{2}\sin 2\Psi\sin^2\Theta\sin 2\Phi$ | Even |
| 6 | $\lvert\overset{(-)}{A}{}_\perp\rvert\lvert\overset{(-)}{A}{}_0\rvert\,\overset{(-)}{\mathcal{E}}{}_{\Im\mathrm{m}}(t,\delta_\perp)$ | $\frac{9}{32\pi}\frac{\sqrt{2}}{2}\sin 2\Psi\sin 2\Theta\cos\Phi$ | Mix |
| 7 | $\lvert\overset{(-)}{A}{}_S\rvert^2\,\overset{(-)}{\mathcal{O}}{}^-(t)$ | $\frac{3}{32\pi}2(1-\sin^2\Theta\cos^2\Phi)$ | Odd |
| 8 | $I_m\lvert\overset{(-)}{A}{}_\parallel\rvert\lvert\overset{(-)}{A}{}_S\rvert\,\overset{(-)}{\mathcal{E}}{}_{\mathfrak{Re}}(t,\delta_\parallel-\delta_S)$ | $\frac{3}{32\pi}2\cos\Psi(1-\sin^2\Theta\cos^2\Phi)$ | Mix |
| 9 | $I_m\lvert\overset{(-)}{A}{}_\perp\rvert\lvert\overset{(-)}{A}{}_S\rvert\sin(\delta_\perp-\delta_S)\,\overset{(-)}{\mathcal{O}}{}^-(t)$ | $\frac{3}{32\pi}\frac{1}{\sqrt{2}}2\sin\Psi\sin^2\Theta\sin 2\Phi$ | Odd |
| 10 | $I_m\lvert\overset{(-)}{A}{}_0\rvert\lvert\overset{(-)}{A}{}_S\rvert\,\overset{(-)}{\mathcal{E}}{}_{\mathfrak{Re}}(t,-\delta_S)$ | $\frac{3}{32\pi}\frac{1}{\sqrt{2}}2\sin\Psi\sin 2\Theta\cos\Phi$ | Mix |

The last column reports the $CP$ parity of each term. The formulae of $\mathcal{O}^\pm$ and $\mathcal{E}_{\Im\mathrm{m}}$ are given by Eqs. (2.35) and (2.40). The coefficient $I_m$ is the integral of the Breit-Wigner resonance mass distribution times the $S$-*wave* component line shape distribution

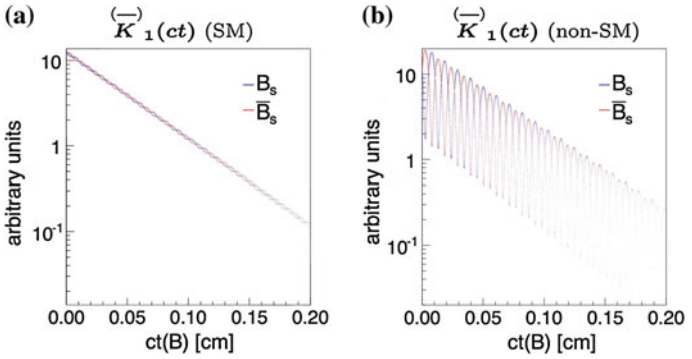


**Fig. 2.7** Evolution of the amplitude $K_1$ for simulated $B_s^0 \to J/\psi K^+K^-$ decays according to Eq. (2.39), as a function of $ct$. *The blue line* refers to initially produced $B_s^0$ mesons and *red line* is for $\bar{B}_s^0$. In **a** the values $\beta_s = 0.02$ and $\Delta\Gamma_s = 0.09\,\text{ps}^{-1}$ (SM point) are used, while in **b** $\beta_s = 0.5$ and $\Delta\Gamma_s = 0.09\cos(2\beta_s^{J/\psi\phi}) = 0.049\,\text{ps}^{-1}$. In both cases, $\Delta m_s = 17.77\,\text{ps}^{-1}$

with the expressions of $\overset{(-)}{K}_i(t)$ and $f_i(\cos\Theta, \Phi, \cos\Psi)$ given in Table 2.5, where the following shorthand in the time-evolution of the interference term between $P$- and $S$-wave with mixed $CP$-parity is introduced:

$$\overset{(-)}{\mathcal{E}}_{\mathfrak{Re}}(t,\alpha) = e^{-\Gamma t}\Bigg(\overset{(-)}{+}\cos\alpha\cos\Delta m_s t \overset{(+)}{-}\sin\alpha\cos 2\beta_s^{J/\psi\phi}\sin\Delta m_s t - \sin\alpha\sin 2\beta_s^{J/\psi\phi}\sinh\frac{\Delta\Gamma_s t}{2}\Bigg), \tag{2.40}$$

where $\alpha$ identifies various combinations of strong phases, as indicated in Table 2.5. Figure 2.7 sketches the evolution of the amplitude $K_1$ ($|A_0(t)|^2$) of the $B_s^0 \to J/\psi K^+K^-$ decay rate in Eq. (2.39), as a function of the decay-length, separately for the $B_s^0$ and the $\bar{B}_s^0$ mesons, assuming the values of $\beta_s^{J/\psi\phi} = 0.02$ and $\Delta\Gamma_s = 0.90\,\text{ps}^{-1}$ in Fig. 2.7a, and $\beta_s^{J/\psi\phi} = 0.5$ and $\Delta\Gamma_s = 0.09\cos(2\beta_s^{J/\psi\phi}) = 0.49\,\text{ps}^{-1}$ in Fig. 2.7b. The value of the oscillation frequency is fixed to the known value $\Delta m_s = 17.77\,\text{ps}^{-1}$ [35], and polarization amplitudes and strong phases are as measured in Ref. [30]. The time-evolution of the decay-amplitude changes significantly for different values of $\beta_s^{J/\psi\phi}$ and $\Delta\Gamma_s$. Specifically, the squared magnitudes of the polarization amplitudes depend on the terms $\cos 2\beta_s^{J/\psi\phi}\sinh(\Delta\Gamma_s t/2)$ and $\sin 2\beta_s^{J/\psi\phi}\sin(\Delta m_s t)$; the former provides sensitivity to $\beta_s^{J/\psi\phi}$ even without distinction of the flavor of the $B_s^0$-meson at production, if $\Delta\Gamma_s$ differs from zero. This last term also explains the different size of the oscillations amplitude between the two cases.

### 2.4.2 Likelihood Symmetries

The decay rate in Eq. (2.39) features some symmetries, i.e., transformations of some of the observables of interest that leave the equations invariant. We first consider the simpler case, where only the $P$-wave is present. Assuming that $B_s^0$ and the $\bar{B}_s^0$ mesons are not distinguished at production, and that they are produced in equal amount (*untagged* sample), then the $B_s^0 \to J/\psi K^+K^-$ and the $\bar{B}_s^0 \to J/\psi K^+K^-$ decay rates are summed. Each oscillation term proportional to $\sin \Delta m_s t$ or $\cos \Delta m_s t$ is canceled out because they appear with opposite sign in the $K_i(t)$ and $\bar{K}_i(t)$ terms, but the rate is still sensitive to $\beta_s^{J/\psi\phi}$ if $\Delta\Gamma_s \neq 0$. The untagged decay rate is invariant under the parameter transformation [34]

$$\begin{cases} \beta_s^{J/\psi\phi} \to \pi/2 - \beta_s^{J/\psi\phi} \\ \Delta\Gamma_s \to -\Delta\Gamma_s \\ \delta_\parallel \to 2\pi - \delta_\parallel \\ \delta_\perp \to \pi - \delta_\perp \end{cases} \tag{2.41}$$

together with the reflection of this transformation with respect to $\beta_s^{J/\psi\phi} = 0$

$$\begin{cases} \beta_s^{J/\psi\phi} \to -\beta_s^{J/\psi\phi} \\ \Delta\Gamma_s \to \Delta\Gamma_s \\ \delta_\parallel \to \delta_\parallel \\ \delta_\perp \to \delta_\perp \end{cases} \quad \text{and} \quad \begin{cases} \pi/2 - \beta_s^{J/\psi\phi} \to -\pi/2 + \beta_s^{J/\psi\phi} \\ -\Delta\Gamma_s \to -\Delta\Gamma_s \\ 2\pi - \delta_\parallel \to 2\pi - \delta_\parallel \\ \pi - \delta_\perp \to \pi - \delta_\perp. \end{cases} \tag{2.42}$$

A four-fold ambiguity is present in the decay rate, with the four equivalent solutions sketched in the $(\beta_s^{J/\psi\phi}, \Delta\Gamma_s)$ plane in Fig. 2.8.

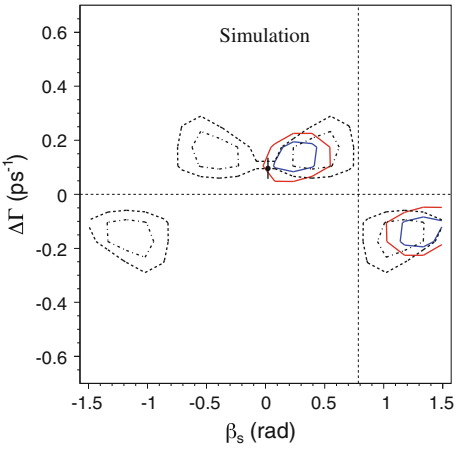


**Fig. 2.8** Example in the $(\beta_s^{J/\psi\phi}, \Delta\Gamma_s)$ plane of the equivalent values of $\beta_s^{J/\psi\phi}$, $\Delta\Gamma_s$, and strong phases, that leave the decay rate invariant. The confidence regions at 68 % C.L. (*blue*) and 95 % C.L. (*red*) for the analysis of a pseudo-experiment with (*bold lines*) and without (*light lines*) using the tagging information

When differences of decay-rates of initially-produced $B_s^0$ and $\bar{B}_s^0$ meson are included through flavor-tagging, the transformations in Eq. (2.42) are no longer symmetries of the decay rate, and only the transformation of Eq. (2.41) leaves the decay rate invariant, resulting in a two-fold ambiguity (with the cancellation of the solutions for $\beta_s^{J/\psi\phi} < 0$ in Fig. 2.8). Tagging allows indeed to access the following terms of the decay rate:

$$\sin 2\beta_s^{J/\psi\phi} \sin(\Delta m_s t) \quad \text{and} \quad \cos 2\beta_s^{J/\psi\phi} \sin(\Delta m_s t), \tag{2.43}$$

that are not present in the untagged rate. The main effect of the tagging in this analysis is to break the $\beta_s^{J/\psi\phi} \to -\beta_s^{J/\psi\phi}$ symmetry (Sect. 2.4.2), removing half of the allowed region in the $(\beta_s^{J/\psi\phi}, \Delta\Gamma_s)$ space. However, the tagging power is not large enough to substantially reduce the uncertainties on the $\beta_s^{J/\psi\phi}$ estimation of the remaining solutions, and each of the four untagged solutions has comparable uncertainties to those on the tagged solutions, as shown in Fig. 2.8, where we compare the results in the $(\beta_s^{J/\psi\phi}, \Delta\Gamma_s)$ plane for tagged and untagged analysis of one simulated samples of $B_s^0 \to J/\psi\phi$ decays. If the tagging power was greater, we would expect the sensitivity to $\beta_s^{J/\psi\phi}$ to be substantially better in the tagged case, and the uncertainties on $\beta_s^{J/\psi\phi}$ to be smaller.

The contribution of the $S$-wave state adds a symmetry transformation in the integrated decay rate

$$\begin{cases} \beta_s^{J/\psi\phi} \to \pi/2 - \beta_s^{J/\psi\phi} \\ \Delta\Gamma_s \to -\Delta\Gamma_s \\ \delta_\parallel \to 2\pi - \delta_\parallel \\ \delta_\perp \to \pi - \delta_\perp \\ \delta_S \to \pi - \delta_S. \end{cases} \tag{2.44}$$

The invariance under tranformation Eq. (2.44) requires the symmetry of the $K^+K^-$ resonances mass shape around the $\phi(1020)$ pole. In the case of asymmetric shapes, the transformation Eq. (2.44) leads to an approximate symmetry, which is more approximate as larger becomes the $S$-wave fraction in the sample. An $S$-wave fraction as expected in CDF data ($\approx$1 %), leaves the decay rate nearly symmetric under the transformation of Eq. (2.44).

These mathematical features of the decay rates lead to difficulties in the likelihood minimization due to the presence of multiple, equivalent minima (Chap. 6). Proper statistical treatment of the resulting features is an important part of this analysis. The statistical reliability of results that are very sensitive to non-SM physics has to be accurately ensured.

**Table 2.6** Experimental status of $B$ mixing observables and corresponding SM predictions in 2010

| Observable | Measurement | Source | SM prediction | References |
|---|---|---|---|---|
| $B_s^0$ system | | | | |
| $\Delta m_s$ (ps$^{-1}$) | $17.78 \pm 0.12$ | HFAG 2010 [25] | $17.3 \pm 2.6$ | [26, 36–39] |
| $\Delta\Gamma_s$ (ps$^{-1}$) | $0.075 \pm 0.035$ | HFAG 2010 [25] | $0.096 \pm 0.039$ | [26, 36–39] |
| $\phi_s$ (rad) | $-0.75^{+0.32}_{-0.21}$ | HFAG 2010 [25] | $-0.036 \pm 0.002$ | [36–41] |
| $a^s_{\rm sl}$ ($10^{-4}$) | $-17 \pm 91^{+14}_{-15}$ | D0 (no $A^b_{\rm SL}$) [42] | $0.29^{+0.09}_{-0.08}$ | [36–41] |
| Admixture of $B^0$ and $B_s$ mesons | | | | |
| $A^b_{\rm SL}$ ($10^{-4}$) | $-78.7 \pm 17.2 \pm 9.3$ | D0 [43] | $-2.0 \pm 0.3$ | [26, 36–39] |

The inclusive same-sign dimuon asymmetry $A^b_{\rm SL}$ is defined in Ref. [43]

## 2.5 Experimental Status

The status of measurements and SM predictions for the mixing observables prior this measurement are summarized in Table 2.6.

The world's average value of the $B_s^0$ mass difference $\Delta m_s$ in Table 2.6 is based on measurements performed at CDF [35] and LHCb [44]. These are all consistent with the SM predictions within sizable theoretical uncertainties. Improving the precision of the SM prediction is desirable to further constrain non-SM physics in $M^s_{12}$, and requires improving the accuracy of lattice QCD evaluations of the decay constant and *bag parameter* (see Ref. [26] and references therein).

The first measurements of the $CP$-violating phase in flavor-tagged $B_s^0 \to J/\psi\phi$ decays was finalized in 2008 by the CDF experiment [45]. It showed a mild, $1.5\sigma$ discrepancy from the SM. Intriguingly the D0 experiment found a similar, and consistent effect [46] a few months later. The combination yielded a $2.2\sigma$ deviation from the SM [47]. This attracted some interest, further enhanced by the like-sign dimuon asymmetry results from the D0 collaboration [43]. Such asymmetry, $A^b_{\rm sl}$, receives contributions from the flavor-specific asymmetries in $B^0$ and $B_s^0$ semileptonic decays, $a^d_{\rm sl}$ and $a^s_{\rm sl}$, respectively. The large value of $A^b_{\rm sl}$ observed by D0, combined with precise determinations of $a^d_{\rm sl}$ from the $B$ factories, suggested an anomalous value of $a^s_{\rm sl}$ and thus an anomalous value of the phase $\phi^s_{12}$, which can be accurately tested using $B_s^0 \to J/\psi\phi$ decays. In 2010, both the CDF and D0 collaborations updated their measurements of $B_s^0 \to J/\psi\phi$ time-evolution using events sample based on 5.2 fb$^{-1}$ and 8 fb$^{-1}$ of integrated luminosity [30, 48]. The results, although consistent with the previous ones, showed an improved agreement with the SM. Also LHCb began to contribute, with a measurement based 340 pb$^{-1}$ of data [44], which already had competitive precision.

## 2.6 Experimental Aspects

The $B_s^0 \to J/\psi(\to \mu^+\mu^-)\phi(\to K^+K^-)$ decay is considered one of the handful of *golden channels* in flavor physics. In addition to allowing access to a key observable, sensitive to a broad class of non-SM physics models and reliably predicted, it offers several experimental advantages. The combined branching fraction is at the $10^{-5}$ level, which makes the collection of significant samples possible in hadron collisions. All final-state particles are charged, thus easier to reconstruct in hadron collisions. In particular, the two muons in the final states originating from the narrow $J/\psi$ resonace, permit to conveniently select online these decays. The fully reconstructed final state provides a strong discrimination against background. This is further enhanced by the presence of two narrow intermediate resonances ($J/\psi$ and $\phi$) whose masses can be used to impose constraints to reduce background. The high multiplicity of tracks in the final state allows a precise determination of the decay vertex position, which is crucial in the study of time evolution.

The measurement of the mixing phase $\beta_s^{J/\psi\phi}$ is conceptually similar to the measurement of the phase $\beta = \arg[(V_{td}V_{tb}^\star)/(V_{cd}V_{cb}^\star)]$ in $B^0 \to J/\psi K_S$ decays, but affected by significant additional experimental difficulties.

On average, a $B_s^0$ meson oscillates four times before decaying, a rate about 15 times faster than the $B^0$ rate. Decay-time resolution is therefore crucial to perform the analysis. The decay-time resolution depends on the relative uncertainty on the decay-length determination. The decay-length absolute uncertainty is controlled in CDF by employing silicon detectors (Sect. 3.2.2). The decay-length value depends on the lifetime of $B_s^0$ mesons and their boost. At CDF the average production momentum of the $B_s^0$ mesons is about 5 GeV/$c$, which yields considerably higher boost than the average boost of $B_s^0$ mesons produced at the $B$-factories that run at the $\Upsilon(5S)$ center of mass energy. This results in $B_s^0$ mesons to fly a significant distance before decaying, which allows a precise determination of the decay-time.

Another complication with respect to the measurement of $\beta$ is the presence of decay amplitudes with different $CP$-eigenstates due to the spin composition of the final states. An angular analysis is required to statistically separate the various components and enhance sensitivity to the mixing phase. An accurate description of the detector effects on reconstructed particle angular distribution is needed.

As in the $B^0 \to J/\psi K_S$ case, sensitivity to the phase is obtained by separately tracking the time evolution of the initially produced $B_s^0$ and $\bar{B}_s^0$ mesons using flavor-tagging. Development and calibration of flavor tagging algorithms is particularly challenging in hadron collider experiments, because of large QCD backgrounds and complicated event topologies. The $\mathcal{O}(5\,\%)$ total tagging power at hadron colliders is low, compared to the $\mathcal{O}(30\,\%)$ tagging power at the $B$ factories. On the other hand, an advantage of the $\beta_s^{J/\psi\phi}$ measurement over the $\beta$ measurement results from the non-zero value of the decay-width difference $\Delta\Gamma_s$. This provides sensitivity to the mixing phase also from non flavor tagged decays, enhancing the statistical power of the event sample.

**Table 2.7** Comparison of key experimental parameters

| Parameter | LHCb ($340\,\text{pb}^{-1}$) [49] | D0 ($8\,\text{fb}^{-1}$) [48] | CDF ($5.2\,\text{fb}^{-1}$) [30] | ATLAS ($4.9\,\text{fb}^{-1}$) [50] |
|---|---|---|---|---|
| $\sigma_t(B_s^0)$ [fs] | ≈50 | ≈100 | ≈90 | ≈100 |
| $\sigma_m(B_s^0)$ [MeV/$c^2$] | ≈7 | ≈30 | ≈10 | ≈7 |
| Effective tagging power | ≈2.1 % | ≈2 % | ≈4.7 % | – |
| Signal yield | 8,300 ($t > 0.3$ ps) | 5,600 | 6,500 | 22,700 |
| $S/B$ at peak | 33/1 ($t > 0.3$ ps) | 1/3 | 2/1 | 3/1 |

The parameters $\sigma_t(B_s^0)$ and $\sigma_m(B_s^0)$ are the mean resolutions on the measurement of the $B_s^0$ decay time and mass, respectively. The effective tagging power is the measurement of the capability to distinguish the production of a $B_s^0$ from a $\bar{B}_s^0$ meson. The symbol $S/B$ stands for the signal to background ratio

Table 2.7 reports a comparison of key experimental parameters of the current experiments.

## 2.7 Analysis Strategy

The measurement of the phase $\beta_s^{J/\psi\phi}$ relies on an analysis of the time-evolution of the $B_s^0 \to J/\psi\phi$ decay in which decays from mesons produced as $B_s^0$ or $\bar{B}_s^0$ are studied independently, and the $CP$-parity of the final state is statistically determined using angular distributions. The data analysis can be dissected in four main steps: (1) selection and reconstruction of the signal event sample; (2) preparation of the analysis tools; (3) fit to the time-evolution; (4) statistical procedure to extract results and uncertainties.

The $B_s^0 \to J/\psi(\to \mu^+\mu^-)\phi(\to K^+K^-)$ event sample is collected by the CDF dimuon online-event selection system [51], which select events enriched in $J/\psi$ decays. In the analysis, these are associated with pairs of tracks consistent with $\phi \to K^+K^-$ decays through a kinematic fit to a common space-point. A total sample corresponding to 10 $\text{fb}^{-1}$ of data, along with a $p\bar{p} \to b\bar{b}$ production cross-section of a few tenths of microbarns, provides an event sample of few thousand $B_s^0$ decays. Precise momentum and vertex reconstruction, along with particle identification capabilities combined in a multivariate selection based on a machine-learning discriminator ensure isolation of an abundant and prominent signal.

Signal contributions in the $B_s^0 \to J/\psi K^+K^-$ final state other than $B_s^0 \to J/\psi\phi$ signal itself are taken into account assuming an $S$-wave state for the $KK$ system.

The sensitivity to $\beta_s^{J/\psi\phi}$ is improved by fitting separately the time evolution of mesons produced as $B_s^0$ from those produced as $\overline{B}_s^0$ and decays occurring in different angular momenta combinations. Hence, prior to fitting the time-evolution of the

decays, the algorithms that identify the $b$ quark content of the strange-bottom meson at production are calibrated on control samples of data. Two algorithms are used for flavor tagging. One of them, the opposite side tagging algorithm has been recalibrated using data corresponding to the final data set. Similarly, the tools for the angular analysis including modeling of detector and selection sculpting are prepared.

The angular, flavor-tagging and decay-time informations are combined in an unbinned multidimensional likelihood fit, the core of the analysis, which uses information from mass, mass uncertainty, decay time, decay-time uncertainty, three-dimensional angular distributions between decay products, and outcome of the flavor tagging algorithms, to extract all the interesting physical parameters, including the phase, the width-difference, the average $B_s^0$ lifetime, the magnitude of the different polarization amplitudes, and a number of technical parameters of lesser importance. The complexity of the fit and some irreducible symmetries of the likelihood make the extraction of proper confidence intervals challenging from the simple fit results. Thorough simulation-based calculations are needed to construct proper confidence regions and finally extract the results.

## References


1. D.H. Perkins, *Introduction to High Energy Physics*, 4th edn. (Cambridge University Press, Cambridge, 2000)
2. G. Aad et al. (ATLAS Collaboration), Observation of a new particle in the search for the Standard Model Higgs boson with the ATLAS detector at the LHC. Phys. Lett. **B716**, 1 (2012) arXiv:1207.7214 [hep-ex]
3. S. Chatrchyan et al. (CMS Collaboration), Observation of a new boson at a mass of 125 GeV with the CMS experiment at the LHC. Phys. Lett. **B716**, 30 (2012) arXiv:1207.7235 [hep-ex]
4. R. Barbieri, ICHEP2012 Physics Highlights, Contribution to the 36th International Conference on High energy Physics, Melbourn, 4–11 July 2012 arXiv:1212.3440 [hep-ph]
5. C. Quigg, Unanswered questions in the electroweak theory. Ann. Rev. Nucl. Part. Sci. **59**, 505 (2009) arXiv:0905.3187 [hep-ph]
6. M.S. Chanowitz, Electroweak symmetry breaking: unitarity, dynamics, experimental prospects. Ann. Rev. Nucl. Part. Sci. **38**, 323 (1988)
7. J. Beringer et al. (Particle Data Group), Review of particle physics. RPP. Phys. Rev. **D86**, 010001 (2012)
8. G. Isidori et al., Flavor physics constraints for physics beyond the standard model. Ann. Rev. Nucl. Part. Sci. **60**, 355 (2010) arXiv:1002.0900 [hep-ph]
9. M. Ciuchini, A. Stocchi, Physics opportunities at the next generation of precision flavor physics. Ann. Rev. Nucl. Part. Sci. **61**, 491 (2011) arXiv:1110.3920 [hep-ph]
10. J. Charles et al. (CKMfitter Group), CP violation and the CKM matrix: assessing the impact of the asymmetric $B$ factories. Eur. Phys. J. **C41**, 1 (2005) hep-ph/0406184. Updated results and plots available at http://ckmfitter.in2p3.fr
11. S. Glashow, J. Iliopoulos, L. Maiani, Weak interactions with Lepton-Hadron symmetry. Phys. Rev. **D2**, 1285 (1970)
12. J. Augustin et al. (SLAC-SP-017 Collaboration), Discovery of a narrow resonance in e+ e− Annihilation. Phys. Rev. Lett. **33**, 1406 (1974)
13. J. Aubert et al. (E598 Collaboration), Experimental observation of a heavy particle. J. Phys. Rev. Lett. **33**, 1404 (1974)

14. F. Abe et al. (CDF Collaboration), Observation of top quark production in $\bar{p}p$ collisions. Phys. Rev. Lett. **74**, 2626 (1995) hep-ex/9503002
15. S. Abachi et al. (DØ Collaboration), Search for high mass top quark production in $p\bar{p}$ collisions at $\sqrt{s} = 1.8$ TeV. Phys. Rev. Lett. **74**, 2422 (1995) hep-ex/9411001
16. H. Albrecht et al. (ARGUS Collaboration), Observation of B0- anti-B0 mixing. Phys. Lett. **B192**, 245 (1987)
17. N. Cabibbo, Unitary symmetry and leptonic decays. Phys. Rev. Lett. **10**, 531 (1963)
18. M. Kobayashi, T. Maskawa, CP violation in the renormalizable theory of weak interaction. Prog. Theor. Phys. **49**, 652 (1973)
19. C. Jarlskog, Commutator of the quark mass matrices in the standard electroweak model and a measure of maximal CP violation. Phys. Rev. Lett. **55**, 1039 (1985)
20. L. Wolfenstein, Parametrization of the Kobayashi-Maskawa matrix. Phys. Rev. Lett. **51**, 1945 (1983)
21. A.J. Buras, M.E. Lautenbacher, G. Ostermaier, Waiting for the top quark mass, $K^+ \to \pi^+\nu\overline{\nu}$, $B^0_{(s)} - \overline{B}^0_{(s)}$ mixing and CP asymmetries in $B$ decays. Phys. Rev. **D50**, 3433 (1994) hep-ph/9403384
22. I. Dunietz et al., In pursuit of new physics with $B_s$ decays. Phys. Rev. D. **63**, 114015 (2001) arXiv:hep-ph/0012219 [hep-ph]
23. P. Ball, R. Fleischer, An analysis of $B_s$ decays in the left-right-symmetric model with spontaneous CP violation. Phys. Lett. B **475**, 111 (2000)
24. I. Dunietz, $B_s - \bar{B}_s$ mixing, CP violation and extraction of CKM phases from untagged $B_s$ data samples. Phys. Rev. **D52**, 3048 (1995) arXiv:hep-ph/9501287 [hep-ph]
25. Y. Amhis et al. (Heavy Flavor Averaging Group), Averages of b-hadron, c-hadron, and tau-lepton properties as of early 2012 (2012) arXiv:1207.1158 [hep-ex]. And updates at http://www.slac.stanford.edu/xorg/hfag
26. A. Lenz, Theoretical update of $B$-mixing and lifetimes (2012) arXiv:1205.1444 [hep-ph]
27. B. Bhattacharya, A. Datta, D. London, Reducing penguin pollution. Int. J. Mod. Phys. **A28**, 1350063 (2013) arXiv:1209.1413 [hep-ph]
28. X. Liu, W. Wang, Y. Xie, Penguin pollution in $B \to J/\psi V$ decays and impact on the extraction of the $B_s - \bar{B}_s$ mixing phase (2013) arXiv:1309.0313 [hep-ph]
29. S. Faller, R. Fleischer, T. Mannel, Precision physics with $B^0_s \to J/\psi\phi$ at the LHC: the quest for new physics. Phys. Rev. **D79**, 014005 (2009) arXiv:0810.4248 [hep-ph]
30. T. Aaltonen et al. (CDF Collaboration), Measurement of the CP-violating phase $\beta_s^{J/\psi\phi}$ in $B^0_s \to J\psi\phi$ decays with the CDF II detector. Phys. Rev. **D85**, 072002 (2012) arXiv:1112.1726 [hep-ex]
31. A. Datta et al., New physics in $b \to s$ transitions and the $B^0_{d,s} \to V_1 V_2$ angular analysis. Phys. Rev. **D86**, 076011 (2012) arXiv:1207.4495 [hep-ph]
32. S. Stone, L. Zhang, $S$-waves and the measurement of CP violating phases in $B^0_s$ decays. Phys. Rev. **D79**, 074024 (2009) arXiv:0812.2832 [hep-ph]
33. S. T'Jampens, Etude de la violation de la symetrie CP dans les canaux charmonium-$K^\star(892)$ par une analyse angulaire complete dependante du temps. Ph.D. thesis, University of Paris VI and VII, 2003, Available as *BABAR* thesis THESIS-03/016
34. F. Azfar et al., Formulae for the analysis of the flavor-tagged decay $B^0_s \to J/\psi\phi$. JHEP **1011**, 158 (2010) arXiv:1008.4283 [hep-ph]
35. A. Abulencia et al. (CDF Collaboration), Observation of $B^0_s - \bar{B}^0_s$ oscillations. Phys. Rev. Lett. **97**, 242003 (2006) arXiv:hep-ex/0609040 [hep-ex]
36. M. Beneke et al., Next-to-leading order QCD corrections to the lifetime difference of B(s) mesons. Phys. Lett. **B459**, 631 (1999) arXiv:hep-ph/9808385 [hep-ph]
37. M. Ciuchini et al., Lifetime differences and CP violation parameters of neutral B mesons at the next-to-leading order in QCD. JHEP **0308**, 031 (2003) arXiv:hep-ph/0308029 [hep-ph]
38. M. Beneke, G. Buchalla, I. Dunietz, Width difference in the $B_s - \bar{B}_s$ system. Phys. Rev. **D54**, 4419 (1996) arXiv:hep-ph/9605259 [hep-ph]
39. M. Beneke, G. Buchalla, A. Lenz, U. Nierste, CP asymmetry in flavor specific B decays beyond leading logarithms. Phys. Lett. **B576**, 173 (2003) arXiv:hep-ph/0307344 [hep-ph]

40. J. Charles et al., Predictions of selected flavour observables within the standard model. Phys. Rev. **D84**, 033005 (2011) arXiv:1106.4041 [hep-ph]
41. A. Lenz, U. Nierste, Theoretical update of $B_s - \bar{B}_s$ mixing. JHEP **0706**, 072 (2007) arXiv:hep-ph/0612167 [hep-ph]
42. V. Abazov et al. (D0 Collaboration), Search for CP violation in semileptonic $B_s$ decays. Phys. Rev. **D82**, 012003 (2010) arXiv:0904.3907 [hep-ex]
43. V. M. Abazov et al. (D0 Collaboration), Measurement of the anomalous like-sign dimuon charge asymmetry with 9 fb$^{-1}$ of $p\bar{p}$ collisions. Phys. Rev. **D84**, 052007 (2011) arXiv:1106.6308 [hep-ex]
44. R. Aaij et al. (LHCb Collaboration), Measurement of the $B_s^0 - \bar{B}_s^0$ oscillation frequency $\Delta m_s$ in $B_s^0 \to D_s^-(3)\pi$ decays. Phys. Lett. **B709**, 177 (2012) arXiv:1112.4311 [hep-ex]
45. T. Aaltonen et al. (CDF Collaboration), First flavor-tagged determination of bounds on mixing-induced CP violation in $B_s^0 \to J/\psi\phi$ decays. Phys. Rev. Lett. **100**, 161802 (2008) arXiv:0712.2397 [hep-ex]
46. V. Abazov et al. (D0 Collaboration), Measurement of $B_s^0$ mixing parameters from the flavor-tagged decay $B_s^0 \to J/\psi\phi$. Phys. Rev. Lett. **101**, 241801 (2008) arXiv:0802.2255 [hep-ex]
47. The CDF and D0 Collaborations, Combination of D0 and CDF results on $\Delta\Gamma_s$ and the CP-violating phase $\beta_s^{J/\psi\phi}$, CDF Note 9787, D0 Note 5928-CONF (2009)
48. V. Abazov et al. (D0 Collaboration), Measurement of the CP-violating phase $\phi_s^{J\psi\phi}$ using the flavor-tagged decay $B_s^0 \to J\psi\phi$ in 8 fb$^{-1}$ of $p\bar{p}$ collisions. Phys. Rev. **D85**, 032006 (2012) arXiv:1109.3166 [hep-ex]
49. R. Aaij et al. (LHCb Collaboration), Measurement of the CP-violating phase $\phi_s$ in the decay $B_s^0 \to J/\psi\phi$. Phys. Rev. Lett. **108**, 101803 (2012) arXiv:1112.3183 [hep-ex]
50. G. Aad et al. (ATLAS Collaboration), Time-dependent angular analysis of the decay $B_s^0 \to J/\psi\phi$ and extraction of $\Delta\Gamma_s$ and the CP-violating weak phase $\phi_s$ by ATLAS (2012) arXiv:1208.0572 [hep-ex]
51. D. Acosta et al. (CDF Collaboration), Measurement of $b$ hadron masses in exclusive $J/\psi$ decays with the CDF detector. Phys. Rev. Lett. **96**, 202001 (2006) hep-ex/0508022

http://www.springer.com/978-3-319-07928-8

CP Violation in {B_s}^0 -> J/psi.phi Decays
Measured with the Collider Detector at Fermilab
Leo, S.
2015, XIII, 137 p. 69 illus., 22 illus. in color., Hardcover
ISBN: 978-3-319-07928-8